PAPER

Check for updates

Transition metal-coordinated graphitic carbon nitride dots as a sensitive and facile fluorescent probe for β-amyloid peptide detection†

Yin Zhang,‡[a] Si Meng,‡[a] Jinhua Ding,[a] Qiwen Peng[a] and Yanyan Yu (ID) *[a,b]

Herein, we developed a sensitive graphitic carbon nitride quantum dot (gCNQD)-based fluorescent strategy for β-amyloid peptide monomer (Aβ) determination down to the ng mL^{-1} level for the first time. To realize this goal, the nanostructured gCNQDs were firstly coordinated with four transition metal ions (Cu^{2+}, Cu^{+}, Fe^{3+}, Zn^{2+}). Our findings showed that the fluorescence (FL) intensity of gCNQDs was quenched in the presence of these metal ions possibly due to the effective chelation with the nitrogen element in gCNQDs and subsequent photoinduced electron transfer (PET) of gCNQDs. The degree of fluorescence quenching was found to be the most intense with the addition of Cu^{2+} and therefore, we selected Cu^{2+} as the quencher for the following Aβ determination. Through binding to Cu^{2+}, the introduction of Aβ unexpectedly induced a further decline of FL intensity. Importantly, on account of different peptide sequences coexisting in the same cerebral system, including $Aβ_{1-11}$, $Aβ_{1-16}$, $Aβ_{1-38}$, $Aβ_{1-40}$ and $Aβ_{1-42}$, their affinities to Cu^{2+} could be reflected by the distinguished declining extent of FL intensity. The possible mechanism of Aβ sensing by the probe was clarified by TEM characterization. The developed fluorescent biosensor was demonstrated to give a wide linear range from 1 to 700 ng mL^{-1} and a low detection limit of 0.18 ng mL^{-1} for $Aβ_{1-42}$. In the end, the proposed fluorescence approach was successfully applied to monitoring of $Aβ_{1-42}$ variations in the cortex and hippocampus of AD rats.

Introduction

Alzheimer's disease (AD) is the most prevalent progressive dementia marked by severe impairments to memory and cognitive functions.[1] Nowadays, this disease has affected more than 18 million individuals worldwide and this number is estimated to increase to 70 million people by 2050.[2] It has been commonly accepted that β-amyloid (Aβ) peptides formed from the cleavage of the amyloid precursor protein play a key role in AD pathogenesis, where the aggregation of monomeric Aβ peptides into insoluble plaque-associated amyloid fibrils would induce a cascade of events that eventually lead to the death of neuronal cells.[3–5] Consequently, the decreased amount of extracellular soluble Aβ monomers in the brain has been considered a key predictor of cognitive impairment in AD.[6,7] In this context, fluorescence, colorimetry, electrochemistry,

surface plasmon resonance (SPR), mass spectrometry (MS) and capillary electrophoresis (CE) have been employed to monitor Aβ species from body fluids and cell media.[8–12] We have also previously reported electrochemical and colorimetric approaches for the quantifications of $Aβ_{1-40/1-42}$ and total Aβ monomers.[13–15] However, direct determination of the Aβ monomer in a complex brain system is still a great challenge, as it is very hard to fulfill the requirements of analytical performance in particular sensitivity, selectivity, and accuracy, available for direct detection in the brain, especially for the intrinsic easy aggregation of Aβ under physiological conditions.

Semiconductor materials are attractive to scientists for their electronic and optoelectronic application, through band-gap engineering in the presence of photon energy, using high-energy conduction band (CB) electrons and photo-generated holes.[16,17] Graphitic carbon nitride (g-C_3N_4) is a typical non-toxic, metal-free and organic polymeric semiconductor, which exhibits outstanding physical and chemical properties and has been universally applied in photosynthesis, electrocatalysis, photodegradation of environmental organic pollutants, bioimaging and biomedicine due to their cut-price and convenient preparation, non-toxicity, high quantum yield, good biocompatibility, and excellent photochemical stability.[18–23] As one of the g-C_3N_4 based nanomaterials, fluorescent graphitic

[a]*Jiangsu Key Laboratory of New Drug Research and Clinical Pharmacy, Xuzhou Medical University, 209 Tongshan Road, Xuzhou 221004, Jiangsu, P.R. China. E-mail: yyyxzmc@163.com*
[b]*Department of Pharmaceutical Analysis, School of Pharmacy, Xuzhou Medical University, 209 Tongshan Road, Xuzhou 221004, P.R. China*
†Electronic supplementary information (ESI) available. See DOI: 10.1039/c8an01620h
‡These authors contributed equally to this work.

carbon nitride quantum dots (gCNQDs) possess multiple advantages including bright fluorescence, good stability, water solubility, biocompatibility, and nontoxicity, making them good candidates in place of traditional QDs.[24,25] Currently, a series of gCNQD-based fluorescent biosensors have been established with enhanced photoresponsive properties for the determination of biothiol,[26] ascorbic acid,[27] zeatin,[28] glucose,[29] *etc*. Typically, it is worth noting that the N-containing structure of gCNQDs provides them the ability to coordinate with metal ions, bringing them into close proximity with each other,[30] which constitutes the basis of metal ion determinations such as Cu^{2+}, Fe^{3+}, and Hg^{2+}.[31-33] However, as far as we know, the utility of gCNQDs as bioprobes for fluorescence detection of important biological species associated with neurodegenerative diseases, such as AD, has only been exploited very little.

In this article, we initially demonstrated the employment of gCNQDs as a highly efficient fluorescent probe for Aβ monomer determination based on metal ion binding-induced fluorescence quenching of gCNQDs. To achieve this goal, gCNQD–metal ion ensembles were designed and prepared, which acted as both the response signal and recognition unit for fluorescence sensing of the Aβ monomer. Cu^{2+}, Cu^+, Fe^{3+} and Zn^{2+} were selected to coordinate with gCNQDs and their differential abilities to quench the FL of gCNQDs were compared, which was possibly due to the aggregations of gCNQDs induced by metal ions. With the addition of the Aβ monomer, owing to their interaction with metal ions, further quenching occurred. Interestingly, the proposed methodology displayed a distinguishable capability to sensitize Aβ species among five Aβ isoforms (Aβ$_{1-11}$, Aβ$_{1-16}$, Aβ$_{1-38}$, Aβ$_{1-40}$ and Aβ$_{1-42}$) under identical conditions by observing the FL changes. On the basis of these properties, a sensitive and selective sensing method based on the FL variations of gCNQD–metal ion ensembles was developed for the detection of Aβ in an AD rat cerebral system.

Experimental

Chemicals and materials

Sodium citrate and urea were bought from the Shanghai Chemical Reagent Company (Shanghai, China). Purified synthetic β-amyloid peptides were obtained from ChinaPeptides Co., Ltd (Shanghai, China). Aβ aggregated forms, including Aβ oligomers and fibrils, were achieved by incubation at 37 °C in PBS with shaking for one and three days, respectively. 1-Ethyl-3-[3-dimethylaminopropyl]carbodiimide hydrochloride (EDC), N-hydroxysulfosuccinimide (NHS), and bovine serum albumin (BSA) were purchased from J&K Scientific Ltd. Copper sulfate ($CuSO_4$) and iron(III) chloride hexahydrate ($FeCl_3 \cdot 6H_2O$) were from Sigma-Aldrich (USA). Phosphate buffer saline (PBS, pH 7.4) containing 8.72 mM Na_2HPO_4, 1.41 mM KH_2PO_4, 136.7 mM NaCl and 2.7 mM KCl was employed as the incubation buffer. Milli-Q ultrapure water was used in all experiments. All reagents were of analytical grade commercially available and used without further purification.

Instruments

All fluorescence spectra were recorded by using a Hitachi F-4600 fluorometer (Hitachi Co. Ltd, Japan). The morphology of gCNQDs was observed on a FEI Tecnai G2 T12 transmission electron microscope (TEM, USA) operating at 120 kV. The TEM specimen was prepared by dropping the sample solutions onto 50 Å carbon coated copper grids with the excess solution being immediately volatilized. UV-vis absorption characterization was performed on a UV-6100 double beam spectrometer (MAPADA, Shanghai). X-ray photoelectron spectroscopy (XPS) investigations were carried out on an ESCALab MKII X-ray photoelectron spectrometer using Mg Kα radiation.

Preparation of gCNQDs

The preparation of gCNQDs was referenced to a reported study.[25] As depicted in the reference, briefly, sodium citrate (0.081 g, 0.28 mmol) and urea (0.101 g, 1.68 mmol) were mixed together and ground to a uniform powder. Then, the mixture was heated to 180 °C in an autoclave for 1 h. The obtained yellowish product was purified by alternative washing with ethanol and centrifugation at 12 000 rpm three times, followed by dialyzing against pure water through a dialysis membrane for 24 h.

Fluorescence quenching of gCNQDs by transition metal ions

For the fluorescence quenching experiment, gCNQD dispersions (5 mg mL^{-1} in water) were firstly activated using 10 mM EDC/NHS for 1 h at 37 °C. After that, various amounts of four metal ions (Cu^{2+}, Cu^+, Fe^{3+} and Zn^{2+}) were individually added to the fixed volume of gCNQD dispersions (220 μL), which was then allowed to be incubated at 37 °C for 1 h. The FL spectra before and after incubation were both collected and compared at 465 nm with excitation at 365 nm.

Aβ determination in buffer solution

Due to the spontaneous aggregation properties of the Aβ monomer, it was quite important to obtain a monomer solution without or with rather little aggregated products. The Aβ monomer stock solution (1 mg mL^{-1}) was prepared according to previous reports with minor modifications.[34] Briefly, 1 mg lyophilized Aβ was dissolved in 1 mL Tris-HCl (25 mM, pH 7.4). Then, it was ultrasonicated for 1 min and centrifuged at 10 000 rpm for 30 min to remove any insoluble particles. When using, the prepared stock solution was diluted to the desired concentration with NaOH (10 mM) and applied to determination immediately. For fluorescence sensing, different concentrations of Aβ standard solutions (50 μL) were added into the above gCNQD–metal ion solutions and incubated for 30 min at room temperature. This procedure was performed in triplicate to investigate the repeatability and stability of this system. Afterwards, the FL intensity of the sensing solution was recorded at 465 nm with excitation at 346 nm. The process of Aβ determination based on this assay is illustrated in Scheme 1.
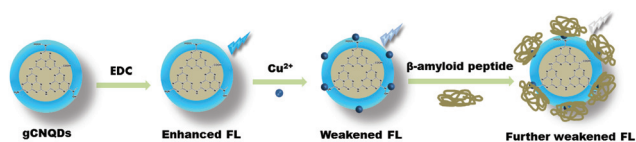
Scheme 1 Schematic illustration of the mechanism of the gCNQD-based fluorescent probe for sensing of the Aβ peptide.

Analysis of cortex and hippocampus homogenates from AD rats

The induction of AD rats was performed according to our previous work.[13] Briefly, male Wistar rats, weighing 100–120 g at the beginning of experiments, were obtained from Shanghai Yisen Biotechnology Co., Ltd. Rats were housed in plastic cages, with food and water available *ad libitum*, and kept under standard environmental conditions (12 h light/dark cycle, 22 °C). All animal experiments were conducted with the approval of the Animal Ethics Committee in Xuzhou Medical University, China. All efforts were made to minimize the number of animals used and their suffering.

D-Galactose (D-gal, Aladdin Reagent Co., Ltd) and ibotenic acid (IBO, Enzo Life Sciences, Inc.) were dissolved in sterile saline and ice PBS (pH 7.4) at their final concentrations of 10 g L^{-1} and 8 g L^{-1}, respectively. Rats were randomly divided into two groups: normal group and D-gal + IBO group (AD model group) (*n* = 15 for each group). The latter group was daily administered with D-gal (50 mg kg^{-1} in 0.5 mL saline, i. p.) for six weeks, which has been demonstrated to be able to produce aging rats.

After D-gal administration, rats in the AD group were anesthetized with sodium pentobarbital (50 mg kg^{-1}, i.p.) and placed on a stereotaxic apparatus (Shenzhen RWD Life Science Co.), with the incisor bar set at 5 mm above the interaural line and appropriately placed holes were drilled through the skull. Stereotaxic coordinates of nucleus basalis magnocellularis (NBM) were set at −1.0 mm posterior and −2.6 mm lateral to bregma and 7.8 mm below from the top of the skull. Bilateral infusions of 1 μL volume of IBO into NBM using a 5 μL Hamilton syringe lasted over a period of 5 min and the needle was left in place for 5 min after completing the infusion. After the surgery, rats were allowed to recover for 45 days before experiments. Cortex homogenates were centrifuged at 4000 rpm for 15 min and the supernatant of the homogenates was used for the following determination.

Samples of cortex and hippocampus homogenates from AD rats (5 μL) were spiked with different concentrations of Aβ$_{1-42}$ (5 μL). The spiked samples were then incubated with the sensing solution (200 μL) for 30 min at room temperature. Subsequently, the FL spectra were recorded. Each experiment was performed in triplicate.

Results and discussion

Structure and optical characterization of the prepared gCNQDs

The gCNQDs used for the peptide determination were characterized by TEM, XPS, XRD, FT-IR, UV–vis absorption, FL emis-

sion and excitation for the morphology, composition and optical property investigation. The typical TEM image of gCNQDs is displayed in Fig. 1A, which revealed a well monodisperse morphology with an average diameter of about 2.7 nm. The lattice fringes of gCNQDs could be clearly observed and the lattice parameter was estimated to be approximately 0.34 nm, which was close to the 002 plane of graphitic carbon nitride.[35] The obtained gCNQDs appeared pale-yellow under white light (inset graph of Fig. 1A). The surface of gCNQDs was abundant in functional groups, including −NH$_2$, −OH and –COOH, which endowed them with high capability to coordinate with multiple metal ions. Likewisely, the surveyed XPS spectra of gCNQDs showed a predominant graphitic C 1s peak at *ca.* 284 eV, an O 1s peak at *ca.* 530 eV and an N 1s peak at *ca.* 400 eV (Fig. 1B). As could be seen from the high resolution C 1s spectrum, two peaks separately centered at 284.6 and 288.0 eV appeared, which could be attributed to graphitic carbon and sp^2 bonded carbon (N–C=N), respectively (Fig. 1C).[30] In the N 1s spectrum, the observed peak at 400.1 eV corresponded to quaternary nitrogen bonded to three carbon atoms in the aromatic cycles (Fig. 1D).[36] The XRD pattern of gCNQDs presented a strong diffraction peak in the (002) plane, which was in accordance with that reported for graphitic carbon nitride (Fig. 2A).[24] FT-IR tests were performed to detect the possible functional groups in gCNQDs. As shown in Fig. 2B, a characteristic peak near 800 cm^{-1} due to the heptazine units of gCNQDs was observed. Bands at 1313 and 1263 cm^{-1} showed the characteristic presence of secondary (2C–N) and tertiary (3C–N) amines. The characteristic bands located between 3000 and 3600 cm^{-1} could be assigned to the N–H stretching and hydrogen-bonding interactions. An intense peak at 1587 cm^{-1} corresponded to the asymmetric
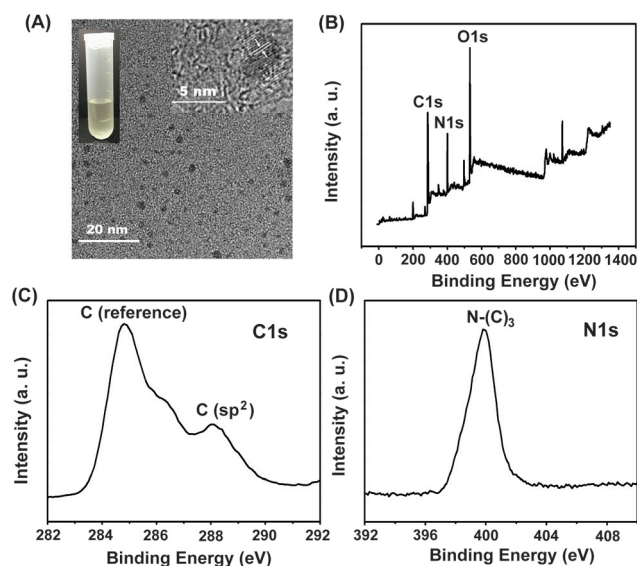

Fig. 1 (A) TEM image of gCNQDs. Insets were the representative HRTEM images of an individual carbon nitride dot and the photograph of gCNQD solution under white light. (B) XPS spectra of gCNQDs. (C and D) The high resolution C 1s (C) and N 1s (D) peaks of gCNQDs.
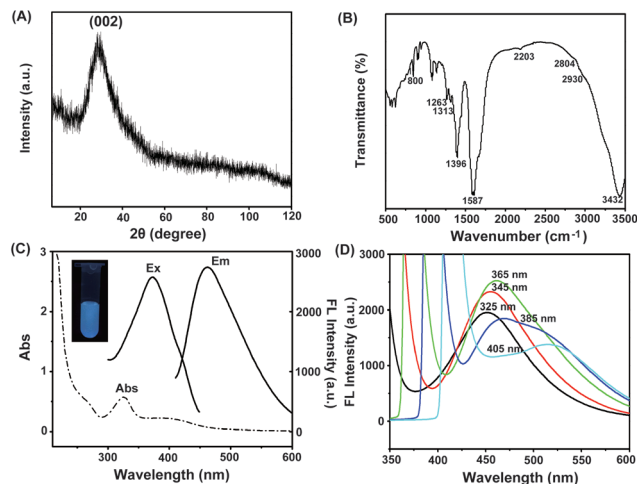
Fig. 2 XRD (A) and FT-IR (B) spectra of gCNQDs. (C) UV-vis and fluorescence spectra of gCNQDs. The inset was the photograph of gCNQD solution under UV irradiation. (D) Fluorescence emission spectra for gCNQDs at different excitation wavelengths.

Fig. 3 Fluorescence responses of gCNQDs in the presence of Cu^{2+} (A), Cu^+ (B), Fe^{3+} (C) and Zn^{2+} (D). The tested concentrations of these metal ions were 0.1, 0.5 and 1.0 μM for Cu^{2+} and 0.5 μM for Cu^+, Fe^{3+} and Zn^{2+}.

stretching vibrations of the carboxylate anion. The peaks at 2203 and 1396 cm^{-1} indicated the existence of N-related bonds.[24,27,34] All these data indicated the successful obtainment of gCNQDs.

To further inspect the optical properties of gCNQDs, UV-vis and fluorescence spectra were recorded (Fig. 2). As shown in Fig. 2C, a maximum absorbance at about 325 nm appeared in the UV−vis spectra, which was in the vicinity of the maximum excitation peak at 365 nm. Under this excitation wavelength, there was a strong emission peak at 465 nm. The inset photograph of the dispersion under UV light (365 nm) exhibited a bright blue color. The gCNQDs displayed an excitation-dependent behavior (Fig. 2D). When the excitation wavelength changed from 325 to 365 nm, the fluorescence intensity firstly increased with the excitation wavelength, and then decreased significantly when the excitation wavelength was larger than 365 nm. The most intense fluorescence peak appeared at 365 nm. Hence, 365 nm was ascertained as the excitation wavelength to excite gCNQDs for fluorescence emission. The prepared gCNQDs could maintain their stability for at least three weeks as no obvious floating or precipitated particles were observed during this period.

Fluorescence response of gCNQDs to metal ions

It has been reported that metal ions could trigger aggregation of carbon-based fluorescent nanomaterials to form chemosensing ensembles and thus a decrease of FL intensity.[37] So next, we explored the fluorescence response of gCNQDs with additions of metal ions. As displayed in Fig. 3A, upon the addition of Cu^{2+} into gCNQD solution, the intensity of fluorescence was found to be obviously quenched and then became stable when the concentration of Cu^{2+} was 0.5 μM. Actually, the feasibility of using gCNQD-based fluorescent
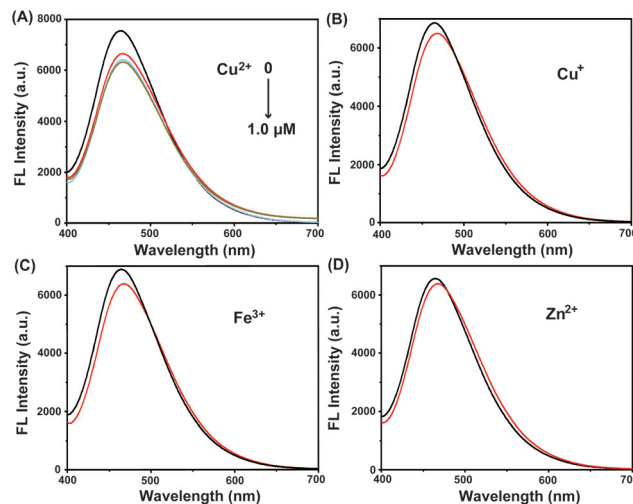
probes for Cu^{2+} detection has been demonstrated in other work, which was based on the effective fluorescence quenching of gCNQDs.[38] Since Cu^{2+} can be chelated by the abundant N in gCNQDs, their interactions brought them close to each other and thus caused the photo-induced electron transfer (PET) from the conduction band (CB) to the complexed Cu^{2+} as the redox potential of Cu^{2+}/Cu^+ lied between the CB and valence band (VB) of gCNQDs. Besides Cu^{2+}, the effects of other transition metal ions that coexist in the cerebral system and involve in modulating Aβ aggregations in the process of AD, such as Cu^+, Fe^{3+}, Zn^{2+}, on the fluorescence of gCNQDs were also investigated. The results in Fig. 3B–D demonstrated that compared with Cu^{2+}, the degrees of fluorescence quenching with the introduction of these three metal ions were much smaller. Among them, Zn^{2+} demonstrated the weakest quenching ability to the FL intensity of gCNQDs, followed by Cu^+ and Fe^{3+}. The distinctive quenching extents were probably due to their diverse interactions with gCNQDs, e.g., the thermodynamic affinity and the chelating efficiency with gCNQDs.[39] Considering the sensitivity, we selected Cu^{2+} as the quencher and designed a gCNQD–Cu^{2+} nanoprobe that could be employed for the following experiments.

Aβ determination based on gCNQD–Cu^{2+} nanoprobe

It has been reported that the Cu^{2+} complexation with the Aβ peptide was responsible for the formation of α-helix conformation, which was favorable for the prevention of peptide accumulation.[40] Hence, based on this interaction, the Aβ peptide was expected to act as a complexing agent for Cu^{2+} and consequently, the quenched fluorescence of the gCNQDs by Cu^{2+} can be basically recovered in the presence of the Aβ peptide. However, as Fig. 4 shows, totally contrary to our expec-
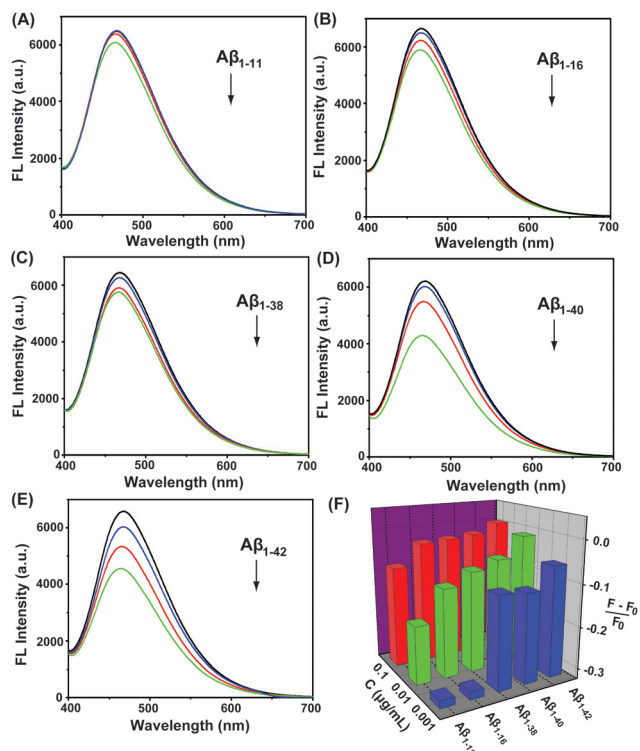
Fig. 4 Fluorescence responses of gCNQD–Cu^{2+} nanoprobe in the presence of Aβ$_{1-11}$ (A), Aβ$_{1-16}$ (B), Aβ$_{1-38}$ (C), Aβ$_{1-40}$ (D), and Aβ$_{1-42}$ (E) with their concentrations of 0.001, 0.01 and 0.1 μg mL^{-1}. (F) The summary of variations of the FL intensity of the probe toward the addition of the five Aβ isoforms at three concentrations.

tation, the FL intensity of the formed gCNQD–Cu^{2+} ensemble was not recovered but continued to decline. Moreover, on account of different peptide sequences coexisting in a rat cerebral system, including Aβ$_{1-11}$, Aβ$_{1-16}$, Aβ$_{1-38}$, Aβ$_{1-40}$ and Aβ$_{1-42}$, their affinities to Cu^{2+} can be reflected by the distinguished declining extent of the FL intensity. For example, when 0.001 μg mL^{-1} Aβ$_{1-11}$ standard solution was introduced into the 0.5 μM Cu^{2+}-contained fluorescent probe and incubated for 30 min, no obvious change in the spectrum was observed. By increasing the concentration of Aβ$_{1-11}$ to 0.01 or even 0.1 μg mL^{-1}, a gradual decrease in the intensity at 465 nm occurred. Similar variations were detected in the incubated solution that contained Aβ$_{1-16}$ or Aβ$_{1-38}$. But compared with Aβ$_{1-11}$, the intensity of the probe was more intense. In particular, as compared with the three Aβ isoforms, additions of Aβ$_{1-40}$ and Aβ$_{1-42}$ into the probe induced a much more intense decrease in the spectral intensity at higher concentrations (e.g., 0.01 or 0.1 μg mL^{-1}). To be better understood, we calculated the $(F - F_0)/F_0$ values for the five Aβ isoforms at three different concentrations, in which F_0 and F represented the FL intensities of the probe before and after incubation with Aβ. The results are displayed in Fig. 4F. In general, the calculated $(F - F_0)/F_0$ values representing the variation extent of the five Aβ isoforms basically increased along with the increase of Aβ concentrations.

Detection mechanism of the strategy toward Aβ

In order to clarify the possible mechanism of Aβ-induced further aggregation of gCNQDs, TEM images were obtained and compared for the morphology observation of the gCNQD–Cu^{2+} nanoprobe in the absence and presence of Aβ. As described above, pure gCNQDs were uniformly dispersed with an average size of about 2.7 nm (Fig. 5A). When Cu^{2+} was added, the original isolated particles began to interconnect with each other, which aroused the aggregation of gCNQDs, along with an increased size of particles (Fig. 5B). In particular, as compared with gCNQD and gCNQD–Cu^{2+} samples, additions of Aβ$_{1-42}$ into the probe induced more densely interconnected particles and increased degree of aggregations (Fig. 5C). To quantitatively better depict the interactions among gCNQDs, Cu^{2+} and Aβ, the specific interconnectivity of the three nanocomposites was calculated. The definition "interconnectivity" was first introduced by the Jiang group,[41] which was defined as the ratio of the total number of interconnected particles divided by the total number of particles involved, see eqn (1), based on the assumption that the particles are spherical with an equal diameter and thus the interconnectivity ratio would vary between 0 and 6 on a planar 2D surface.

$$\text{Interconnectivity} = \sum \text{number of interconnected particles}/ \sum \text{number of particles}$$

(1)

As could be seen from Fig. 5D, with the subsequent interaction between Cu^{2+} and Aβ, the particle interconnectivity of gCNQDs increased from 0.8 to 3.9, consistent with the TEM results. These observations corresponded well with the above-mentioned fluorescence results that the FL intensity gradually decreased followed by additions of Cu^{2+} and Aβ step by step. The possible mechanism for the observed further aggregation and quenching of gCNQDs with the addition of Aβ could be due to the similar coordination ability of Cu^{2+} with the functional groups of gCNQDs and Aβ. Consequently, acting as linking bridges, Cu^{2+} and Aβ brought more dots close to each other and thus a more dense aggregation occurred.[42] Moreover, a control experiment was also done to test the fluorescence response of gCNQDs toward Aβ without preliminary addition of Cu^{2+}. As could be seen from Fig. S2,† additions of Aβ solutions (0.01 and 0.07 μg mL^{-1}) didn't induce obvious fluorescence intensity changes of gCNQDs. On surface passivation by oxygen-rich functional groups, the gCNQDs were all negatively charged. When gCNQDs encountered Aβ that was also negatively charged, Coulomb repulsions happened between them, which prevented the aggregations of gCNQDs and quenching of FL intensity. This result further confirmed the proposed mechanism that it was due to the existence of Cu^{2+} in the sensing system and the interaction between Cu^{2+} and Aβ, and further aggregation and quenching of gCNQDs could occur.
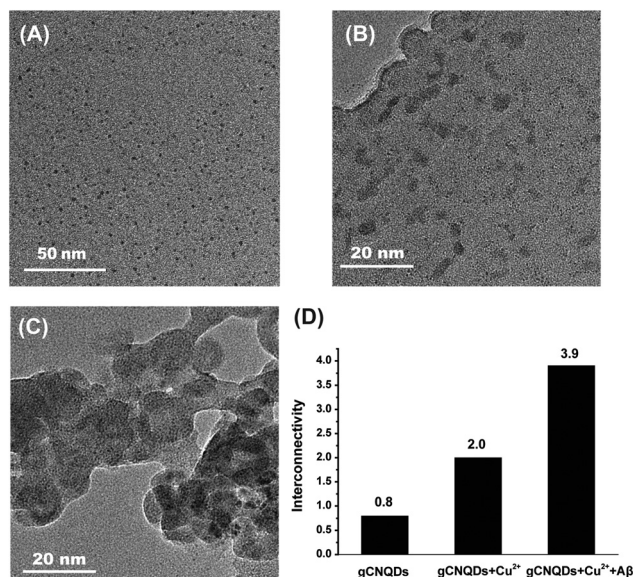
Fig. 5 TEM images of gCNQDs (A), gCNQD–Cu^{2+} nanoprobe in the absence (B) and presence of $A\beta_{1-42}$ (C). (D) Calculated interconnectivity of the three nanocomposites.

Sensitivity of the gCNQD–Cu^{2+} nanoprobe on Aβ determination

On the basis of the above results, a rapid, sensitive sensing method based on the fluorescence change of gCNQDs–Cu^{2+} was developed for the detection of Aβ. Fig. 6A shows the FL spectra of the probe upon additions of different concentrations of $A\beta_{1-42}$. It was observed that the FL intensity at 465 nm gradually decreased with increasing $A\beta_{1-42}$ concentration and finally reached a plateau at 700 ng mL^{-1}, revealing that the FL intensity of the system was sensitive to $A\beta_{1-42}$. Meanwhile, the plot in the inset of Fig. 6A exhibited a good linear relationship between FL intensities and the logarithm of $A\beta_{1-42}$ concentrations in the wide range of 1–700 ng mL^{-1}. The regression equation was $y = -0.02-0.08 \log x$, with a correlation coefficient (R^2) of 0.9907, where y and x denoted the fluorescence variation $(F - F_0)/F_0$ and $A\beta_{1-42}$ concentration, respectively. The corresponding detection limit (LOD) for $A\beta_{1-42}$ estimated according to the 3σ rule, where σ represented the standard deviation of the blank signal, was found as 0.18 ng mL^{-1} (roughly equal to 45 pM) at 3σ. This value was more or less similar or superior to our previously established electrochemical[13,14] and colorimetric methods[15] and other reported assays,[8,11,33] which indicated that the established fluorescent approach held great potential for Aβ determination in a biological matrix.

Selectivity, reproducibility and stability investigation

Besides a good line fit in a wide linear range, the selectivity of the approach on Aβ determination was also examined. In general, Cu^{2+} was reported to be easily bound to some amino acids and other endogenic substances.[43] Therefore, amino
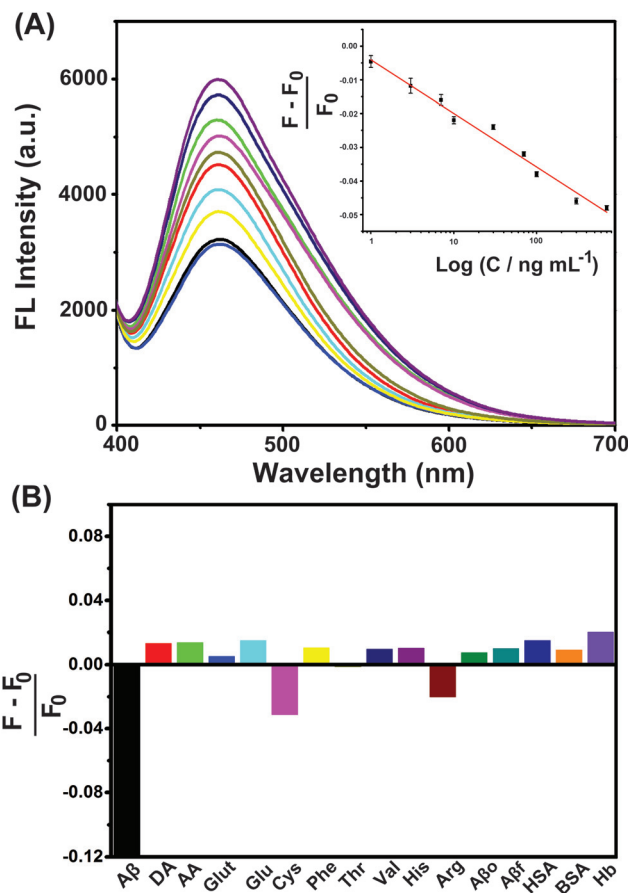

Fig. 6 (A) Fluorescence responses of gCNQD–Cu^{2+} nanoprobe in the presence of increasing concentrations of $A\beta_{1-42}$: 0, 1, 3, 7, 10, 30, 70, 100, 300, 700 ng mL^{-1}. Inset was the linear relationship between the $(F - F_0)/F_0$ values and logarithm of $A\beta_{1-42}$ concentrations. (B) Fluorescence responses of gCNQD–Cu^{2+} nanoprobe in the presence of potential interferences. The amino acids were all 5 μM for cysteine (Cys), phenylalanine (Phe), arginine (Arg), threonine (Thr), valine (Val) and histidine (His). Concentrations of the tested endogenic species were 10 μM for ascorbic acid (AA), dopamine (DA), glutamate (Glut) and uric acid (UA), 1 mM for glucose (Glu), 10 μM for human serum albumin (HSA), 5 μM for bovine serum albumin (BSA) and hemoglobin (Hb). Aβo and Aβf referred to Aβ oligomers and fibrils and their concentrations were 0.1 μg mL^{-1}.

acids including cysteine (Cys), phenylalanine (Phe), threonine (Thr), valine (Val), histidine (His), arginine (Arg) and common endogenic compounds such as ascorbic acid (AA), dopamine (DA), glutamate (Glut) and glucose (Glu) were selected as the potential interferences in Aβ detection. It could be seen from Fig. 6B that the majority of inspected interferences had quite a different effect on the fluorescence of gCNQDs–Cu^{2+} in comparison with the Aβ monomer, which tended to slightly enhance the FL intensity rather than to quench it. Moreover, considering the coexistence of the Aβ monomer, oligomer and fibril in the same cerebral system, we also checked the FL changes in the gCNQD based fluorescent probe in the presence of Aβ oligomers and fibrils under identical conditions. Aβ oligomers and fibrils were prepared by incubation at 37 °C in PBS with shaking for one and three days, respectively. Their

presence was characterized by TEM. As shown in Fig. S1A,† mostly global particles corresponding to the oligomeric form and limited mature fibrils were observed when the Aβ monomer was incubated for one day. By increasing the incubation time, typical amyloid fibrils were predominant in the image (Fig. S1B†). The result from Fig. 6B suggested that these two Aβ aggregates could also not interfere with Aβ monomer detection. In cases of Cys and Arg, although their introductions induced similar changes in intensity to the Aβ monomer, their concentrations in AD rat brains were lower than their present concentrations (5 μM). So we could infer that the interference of Cys and Arg would be reduced in real sample detection, which contained a lower concentration. To test this statement, we reduced the concentration of Cys to be 2 μM and investigated its fluorescence response. It was found that the response signal was cut more than in half compared with that of 5 μM Cys (data not shown). Therefore, we believed that Cys and Arg would not produce significant interferences in Aβ detection. All this evidence indicated the excellent selectivity of the present method for the Aβ monomer against endogenous compounds in the cerebral system and could be further used to detect the Aβ monomer in bio-systems.

In addition, the intra- and inter-day precisions of the proposed methodology were respectively analyzed by repeated measurements of the same concentration of Aβ in four replicates on the same day and consecutively for three days. And the relative standard deviations (RSD) were evaluated to be 1.7% and 5.8%, indicating acceptable repeatability and reproducibility for the determination of Aβ. The nanoprobe also displayed reasonable stability for the analyte, in which approximately 84% of the FL intensity was retained after the probe was stored in 4 °C for three weeks.

Real sample determination

The gCNQD based fluorescent probe offered highly selective and sensitive detection for the Aβ$_{1-42}$ monomer in aqueous solution, which was appropriate for real sample monitoring. A standard addition method was applied to estimate the level variations of Aβ$_{1-42}$ in the cortex and hippocampus from the AD rat brain. Various amounts of Aβ$_{1-42}$ were firstly spiked with cortex and hippocampus homogenates and then added into Cu^{2+}-contained PBS buffer. As listed in Table S1,† the recoveries of these measurements were in the range of 80%–112% under the optimal conditions, indicating that this method was reliable and practical.

Conclusions

To sum up, an efficient approach was exploited for Aβ monomer determination through the design of a fluorescent probe based on Cu^{2+}-coordinated gCNQDs, which took advantage of the strong fluorescence emission properties and large surface area of gCNQDs. The coordination with Cu^{2+} efficiently quenched the FL intensity of gCNQDs at 465 nm *via* aggregation of gCNQDs. The resulting gCNQD–Cu^{2+} ensemble was

capable of interacting with Aβ, leading to a further decrease in the fluorescence emission and thus provided a sensitive platform for Aβ$_{1-42}$ monitoring down to ng mL^{-1}. Importantly, the decrease extent was differentiable depending on the sequence of Aβ. Moreover, the gCNQD-based fluorescence sensing system has been successfully used for the monitoring of Aβ$_{1-42}$ variations in the cortex of AD rats. The proof-of-concept experiment demonstrated that gCNQDs could potentially serve as a reliable alternative for sensitive clinical analysis of important biomarkers related to neurodegenerative diseases such as AD, Parkinson's disease and Huntington's disease.

Conflicts of interest

There are no conflicts to declare.

Acknowledgements

Notes and references

1 J. L. Cummings and G. Cole, *JAMA, J. Am. Med. Assoc.*, 2002, **287**, 2335–2338.
2 Y. Chen, H. Z. Lin, J. Zhu, K. Gu, Q. Li, S. Y. Yu, X. Lu, R. X. Tan, Y. Q. Pei, L. Wu, Y. Y. Bian and H. P. Sun, *RSC Adv.*, 2017, **7**, 33851–33867.
3 D. J. Selkoe, *J. Neuropathol. Exp. Neurol.*, 1994, **53**, 438–447.
4 W. Yang, Y. Wong, O. T. Ng, L. P. Bai, D. W. Kwong, Y. Ke, Z. H. Jiang, H. W. Li, K. K. Yung and M. S. Wong, *Angew. Chem., Int. Ed.*, 2012, **51**, 1804–1810.
5 A. A. Reinke, P. M. U. Ung, J. J. Quintero, H. A. Carlson and J. E. Gestwicki, *J. Am. Chem. Soc.*, 2010, **132**, 17655–17657.
6 A. Nordberg, *Neuropsychologia*, 2008, **46**, 1636–1641.
7 H. E. Wong, W. Qi, H. M. Choi, E. Fernandez and I. Kwon, *ACS Chem. Neurosci.*, 2011, **2**, 645–657.
8 N. Xia, L. Liu, M. G. Harrington, J. Wang and F. Zhou, *Anal. Chem.*, 2010, **82**, 10151–10157.
9 T. E. Golde, C. B. Eckman and S. G. Younkin, *Biochim. Biophys. Acta*, 2000, **1502**, 172–187.
10 L. A. Munishkina and A. L. Fink, *Biochim. Biophys. Acta*, 2007, **1768**, 1862–1885.
11 R. Picou, J. P. Moses, A. D. Wellman, I. Kheterpal and S. D. Gilman, *Analyst*, 2010, **135**, 1631–1635.
12 T. Hu, C. X. Chen, G. M. Huang and X. R. Yang, *Sens. Actuators, B*, 2016, **234**, 63–69.

13 Y. Y. Yu, L. Zhang, C. L. Li, X. Y. Sun, D. Q. Tang and G. Y. Shi, *Angew. Chem., Int. Ed.*, 2014, **53**, 12832–12835.

14 Y. Y. Yu, X. Y. Sun, D. Q. Tang, C. L. Li, L. Zhang, D. X. Nie, X. X. Yin and G. Y. Shi, *Biosens. Bioelectron.*, 2015, **68**, 115–121.

15 Y. Y. Yu, L. Zhang, X. Y. Sun, C. L. Li, Y. Qiu, H. P. Sun, D. Q. Tang, Y. W. Liu and X. X. Yin, *Chem. Commun.*, 2015, **51**, 8880–8883.

16 D. Nandi, A. Taher, R. Ul Islam, S. Siwal, M. Choudhary and K. Mallick, *R. Soc. Open Sci.*, 2016, **3**, 160580–160592.

17 H. J. Kim and J. H. Lee, *Sens. Actuators, B*, 2014, **192**, 607–627.

18 H. Li, M. M. Yang, J. Liu, Y. L. Zhang, Y. M. Yang, H. Huang, Y. Liu and Z. H. Kang, *Nanoscale*, 2015, **7**, 12068–12075.

19 L. S. Lin, Z. X. Cong, J. Li, K. M. Ke, S. S. Guo, H. H. Yang and G. N. Chen, *J. Mater. Chem. B*, 2014, **2**, 1031–1037.

20 R. Chen, J. F. Zhang, Y. Wang, X. F. Chen, J. A. Zapien and C. S. Lee, *Nanoscale*, 2015, **7**, 17299–17305.

21 H. Wan, Y. Zhang, W. B. Zhang and H. F. Zou, *ACS Appl. Mater. Interfaces*, 2015, **7**, 9608–9618.

22 S. Patnaik, S. Martha and K. M. Parida, *RSC Adv.*, 2016, **6**, 46929–46951.

23 H. Q. Zhang, Y. H. Huang, X. H. Lin, F. F. Lu, Z. S. Zhang and Z. B. Hu, *Sens. Actuators, B*, 2018, **255**, 2218–2222.

24 H. Abdolmohammad-Zadeh and E. Rahimpour, *Sens. Actuators, B*, 2016, **225**, 258–266.

25 J. Zhou, Y. Yang and C. Y. Zhang, *Chem. Commun.*, 2013, **49**, 8605–8607.

26 Q. J. Lu, H. Y. Wang, Y. L. Liu, Y. X. Hou, H. T. Li and Y. Y. Zhang, *Biosens. Bioelectron.*, 2017, **89**, 411–416.

27 O. J. Achadu and T. Nyokong, *Anal. Chim. Acta*, 2017, **991**, 113–126.

28 Y. Wang, Y. L. Zhou, L. Xu, Z. W. Han, H. S. Yin and S. Y. Ai, *Sens. Actuators, B*, 2018, **257**, 237–244.

29 S. Liu, J. Tian, L. Wang, Y. Luo and X. Sun, *RSC Adv.*, 2012, **2**, 411–413.

30 Y. Xiao, Y. H. Sheng, J. Zhou, M. M. Chen, W. Wen, X. H. Zhang and S. F. Wang, *Analyst*, 2017, **142**, 2617–2623.

31 S. Zhang, J. Li, M. Zeng, J. Xu, X. Wang and W. Hu, *Nanoscale*, 2014, **6**, 4157–4162.

32 S. Chen, N. Hao, D. Jiang, X. Zhang, Z. Zhou, Y. Zhang and K. Wang, *J. Electroanal. Chem.*, 2017, **787**, 66–71.

33 G. Shiravanda, A. Badiei and G. M. Ziarani, *Sens. Actuators, B*, 2017, **242**, 244–252.

34 C. K. Wang, D. J. Liu and Z. X. Wang, *Chem. Commun.*, 2012, **48**, 8392–8394.

35 Y. Yin, Y. M. Zhang, T. L. Gao, T. Yao, J. C. Han, Z. B. Han, Z. H. Zhang, Q. Wu and B. Song, *Mater. Chem. Phys.*, 2017, **194**, 293–301.

36 S. B. Yang, Y. J. Gong, J. S. Zhang, L. Zhan, L. L. Ma, Z. Y. Fang, R. Vajtai, X. C. Wang and P. M. Ajayan, *Adv. Mater.*, 2013, **25**, 2452–2456.

37 C. Q. Ding, A. W. Zhu and Y. Tian, *Acc. Chem. Res.*, 2014, **47**, 20–30.

38 J. Q. Tian, Q. Liu, A. M. Asiri, A. O. Al-Youbi and X. P. Sun, *Anal. Chem.*, 2013, **85**, 5595–5599.

39 A. P. de Silva, H. Q. N. Gunaratne, T. Gunnlagsson, A. J. M. Huxley and C. P. McCoy, *Chem. Rev.*, 1997, **97**, 1515–1566.

40 Y. Y. Yu, P. Wang, X. D. Zhu, Q. W. Peng, Y. Zhou, T. X. Yin, Y. X. Liang and X. X. Yin, *Analyst*, 2018, **143**, 323–331.

41 Y. Y. Yu, Y. Yang, H. Gu, T. S. Zhou and G. Y. Shi, *Biosens. Bioelectron.*, 2013, **41**, 511–518.

42 S. Sun, K. Jiang, S. H. Qian, Y. H. Wang and H. W. Lin, *Anal. Chem.*, 2017, **89**, 5542–5548.

43 R. Miao, L. X. Mu, H. Y. Zhang, G. W. She, B. J. Zhou, H. T. Xu, P. F. Wang and W. S. Shi, *Nano Lett.*, 2014, **14**, 3124–3129.